Acquisition duration in resting-state arterial spin labeling. How long is enough?

Corentin Vallée, Pierre Maurel, Isabelle Corouge, Christian Barillot

Acquisition duration in resting-state arterial spin labeling. How long is enough?

Corentin Vallée[a,b], Pierre Maurel[a], Isabelle Corouge[a], Chrisitan Barillot[a]

[a] *Univ. Rennes, Inria, CNRS, IRISA, Inserm, Empenn U1228, Campus de Beaulieu, F-35042 Rennes, France*
[b] *Corresponding author: cvallee@irisa.fr*

Abstract

Resting-state Arterial Spin Labeling (rs-ASL) is a rather confidential method compared to resting-state BOLD but drives great prospects with respect to potential clinical applications. By enabling the study of CBF maps, rs-ASL can lead to significant clinical subject-scaled applications as CBF is a biomarker in neuropathology. An important parameter to consider in functional imaging is the acquisition duration. Despite directly impacting practicability and functional networks representation, there is no standard for rs-ASL. Our work here focuses on strengthening the confidence in ASL as a rs-fMRI method and on studying the influence of the acquisition duration. To this end, we acquired a long rs-ASL sequence and assessed the quality of typical functional brain networks quality over time compared to gold-standard networks. Our results show that after 14 min of duration acquisition, functional networks representation can be considered as stable.

Keywords: Arterial Spin Labeling, Resting-state, Acquisition duration

1. Introduction

Functional MR imaging (fMRI) builds the links between location and function in the brain. The two main sub-domains in fMRI are task-based fMRI and resting-state fMRI. In task-based fMRI, a functional location is considered to be where the acquired signal matches with the task guidelines given to the subject. In resting-state fMRI, as no task is given, the focus is on fluctuations in voxels time-series induced by spontaneous neural activations. Similarities in these time-series in different areas have shown to be not random, but matching function of

the brain (Biswal et al., 1995). These similarities define the *functional connectivity* of the brain and show the underlying cerebral architecture organized into functional specialized units communicating with each other. Resting-state functional imaging aims to identify functional areas of the brain and depict how they interact outside any structural connectivity consideration (Van den Heuvel and Hulshoff Pol, 2010) . Healthy and diseased subjects differ in functional networks cartography and in the intensity of functional connectivity for major disorders such as Parkinson's disease (Gao and Wu, 2016), Alzheimer's disease (Agosta et al., 2012), severe depression (Craddock et al., 2009) or schizophrenia (Lynall et al., 2010).

Another subdivision in fMRI concerns the way the signal is obtained. The two major techniques are Blood Oxygen Level Dependent (BOLD) fMRI and functional Arterial Spin Labeling (fASL). Based on neurovascular coupling effects, BOLD techniques rely on the local signal variation induced by the neuron consumption of blood oxygen. Arterial Spin Labeling (ASL) is an MRI perfusion technique which uses magnetically labeled arterial water protons as an endogenous tracer. An inversion pulse labels the inflowing blood and after a delay called post-labeling delay, a labeled image of the volume of interest is acquired. The subtraction of the labeled image from a control image, i.e., non labeled, reflects the quantity of spins that have perfused the imaged volume, producing what is commonly called a perfusion-weighted (PW) image.

The PW map can be used to quantify the cerebral blood flow (CBF) under some assumptions (Buxton et al., 1998; Borogovac and Asllani, 2012). The quantification of CBF is the main advantage of ASL over BOLD. Indeed, the latter provides an indirect and non-quantitative measurement of neural activity, as it results from a combination of variations in CBF, cerebral blood volume and cerebral metabolic rate of oxygen. While the pathologies mentioned above were studied with BOLD, ASL allows to study a new set of pathologies with fMRI, such as acute stroke (Wang et al., 2012) or chronic fatigue syndrome (Boissoneault et al., 2016) since CBF abnormalities can characterize pathologies.

The main drawback of ASL is its lower signal-to-noise ratio compared to BOLD fMRI. The repetition time (TR) is also twice to three times higher in fASL compared to BOLD fMRI, which impacts its temporal resolution. Furthermore, ASL can be implemented through numerous MRI sequences and meta-analyses can be difficult to set up, for ASL shows a high sequence parameter dependency(Grade et al., 2015; Mutsaerts et al., 2015). Nevertheless consensus seems to overcome with years (Alsop et al., 2015). Predominant in clinical usage and in academic research, BOLD is still considered as the gold standard in fMRI.

However, as it provides quantification of CBF, ASL can be a serious contender to BOLD when it comes to pathologies evaluation, especially for Alzheimer's disease (Alsop et al., 2010; Wolk and Detre, 2012; Zhang et al., 2016). The absence of contrast agent injection makes ASL well suited for longitudinal studies, particularly for pediatric population or for population with poor venous access or contrast agent contraindication.

The acquisition duration is an important parameter in an rs-fMRI study with strong practical consequences. Most current studies work with a duration from 8 min to 13 min and a TR from 3 s to 4 s (i.e. 120 to 260 images). Intuitively, one would assume the longer the duration, the better the sampling of the signal correlation across the brain and thus the better the acquisition. But this requires to define what "better" actually means and does not consider the practical questions of clinical implementation and subject resting-state upholding. To the best of our knowledge, only few papers studied the influence of duration in rs-BOLD (Birn et al., 2013; Bouix et al., 2017), whereas in rs-ASL, it has not been explored yet. In this work, we first focus on the feasibility of detecting functional connected regions of the brain from rs-ASL. We remain as close as what a typical investigator of rs-ASL would experience by implementing usual sequence, processing and functional networks detection methods. We then assess a trend over the duration influence on rs-ASL detected networks quality: we do not directly assess whether an acquisition is good at a given time, but rather how it evolves with longer durations. After describing the scores used and the modeling approach, an in-depth analysis for the Default-Mode Network (DMN) will be presented in order to illustrate scores evolution on the most typical resting-state network. Finally, we will show results for all the functional networks under consideration and discuss an optimal sequence duration in rs-ASL.

2. Material

2.1. Subjects

Seven healthy male right-handed subjects aged from 21 to 28 years (23.5 yo$\pm$2.5) were involved in this study. All subjects gave informed written consent before participating in the study. We have maintained the homogeneity of the population in order to limit the influence of factors such as gender or age.

2.2. MR Acquisitions

The subjects were scanned on a 3.0T whole body Siemens MR scanner (Magnetom Verio, Siemens Healthcare, Erlangen, Germany) with a 32-channel

head coil. A 3D anatomical T1-weighted MP2RAGE image was acquired for each subject. The resting-state ASL imaging was performed using a 2D EPI pseudo-continuous (pCASL) sequence. Subjects were asked to keep their eyes closed, to relax (mind-wandering) without falling asleep. We used the most common parameters reported in the literature: TR = 3500 ms, FoV = 224 x 224 mm^2, TE = 12 ms, LD = 1500 ms and a 1250 ms post-labeling delay (PLD). Volumes were made of 24 slices of 64×64 voxels with 5 mm slice thickness with 20% gap for a total resolution of $3.5 \times 3.5 \times 6\,mm^3$. The number of volumes was 420 for a total duration of 24 min 30 s. For the 1250 ms PLD, we chose a balance between a longer duration, about 1800 ms, recommended to optimize the quality of the CBF estimate (Alsop et al., 2015; Chen et al., 2015), and a shorter duration, 600 ms, which seems to give a better functional representation (Liang et al., 2012, 2014). We kept the PLD quite long as the main advantage of ASL is ultimately to compute CBF although we will focus on functional areas representation in this paper.

2.3. Data preprocessing

Each of the subjects' raw acquisition is then divided into 46 sub-series. The duration of these sub-series ranges from nearly 2 min (34 volumes) to 24 min 30,s (420 volumes) with a time step of 30 s. For the sake of simplicity, we will only mention rounded durations hereafter. All these subdivisions are made *before* any preprocessing: the preprocessing is done independently on each sub-series. For the preprocessing steps and their parameters we chose the most common ones found in bibliography. All steps are shown in Figure 1.

3. Methods

3.1. Detecting networks with Seed-Based Analysis

To obtain the mapping of invidivual functional networks, we rely on seed-based analysis (SBA) (Van den Heuvel and Hulshoff Pol, 2010). The principle of this method, the first to be proposed to define functional connectivity (Biswal et al., 1995), is quite straightforward. Considering a similarity measure (usually linear correlation, but many contenders exist (Zhou et al., 2009)), SBA builds functional areas by gathering voxels which exhibit a matching signal, in the sense of the chosen measure, to that of a ROI, called the seed in this context. Even if SBA is a very polymorphic modeling method, we use its most common form in our work. Hence we consider linear correlation as the similarity measure and use a set of 20 single voxels as seeds. Seeds are spread in the expected location of

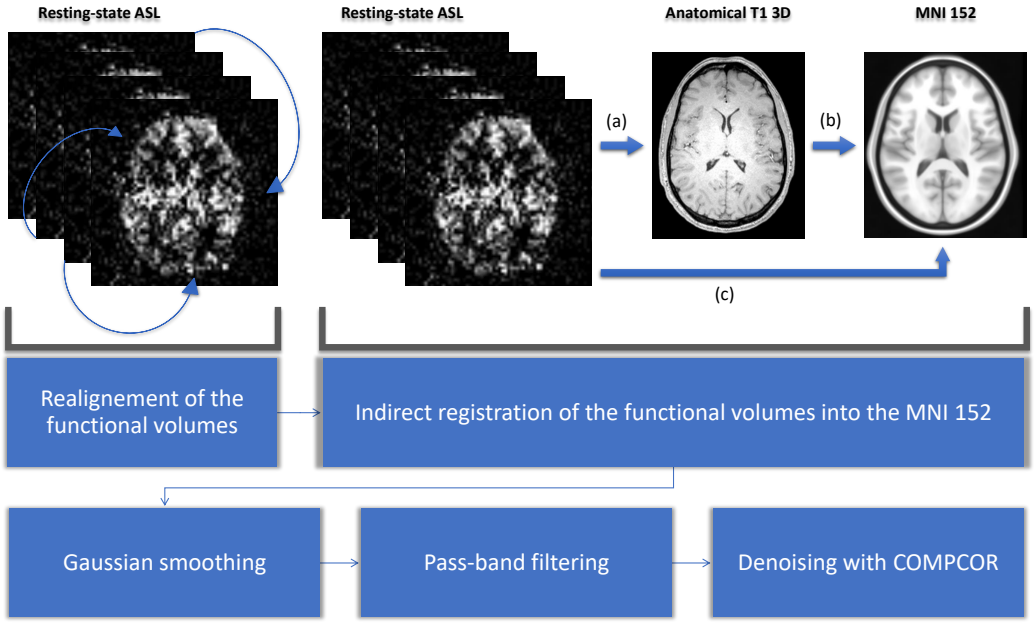

Figure 1: Preprocessing steps of the rs-ASL images. Preprocessing starts with the realignment of the functional data. All the functional volumes are registered with the first one. Second step is the indirect normalization of the functional volumes. It starts with registration of the functional on the anatomical T1 3D (a). Then comes the registration of the anatomical on the MNI 152 template (b). Finally, transformations of (a) and (b) are composed to register functional on MNI (c). We then used Gaussian smoothing with typical 6 mm kernel and pass-band filtering with a range from 0.005 Hz to 0.1 Hz. Final denoising was made with COMPCOR. (Behzadi et al., 2007)

six usual functional networks: DMN, Sensori-motor, Language, Salience, Visual and Cerebellum. The exact positions of the seeds in the MNI152 space are provided in the appendix section and were suggested by the CONN toolbox. To build a functional map for each seed, we statistically test whether the signal between the seed and a candidate voxel is positively correlated with a risk of 1% FWER-corrected. This is a tough conservative testing compared to most of rs-ASL (even fMRI in general) studies, but we agree with the recommendation of (Eklund et al., 2016) on false positive underestimation in fMRI.

3.2. Evaluation scores

In order to investigate a trend afterwards, the individual functional maps must be compared to a reference. For that purpose, we rely on the Multi-

Subjects Dictionary Learning atlas (MSDL) by (Varoquaux et al., 2011). MSDL is an atlas of 17 resting-state functional networks containing our 6 networks of interest, and from which our seeds are independent. The key idea is to have functional maps close to what an expert would expects to observe when looking for the typical functional areas investigated here. To study the quality of the detected networks as a function of the acquisition duration, we evaluate the overlap between the SBA estimated functional maps and the MSDL references (simply called "reference" hereafter) through two measures: the Jaccard's index and the area under curve (AUC).

Let $\mathbb{E}$ be a set, let $(v_i)_{i\leqslant k\in\mathbb{N}}$ be observations in $\mathbb{E}$ and $(M_1; M_2) \in \{0; 1\}^{\mathbb{E}} \times \{0; 1\}^{\mathbb{E}}$ binary categorical variables. Let A,B,C,D be four sets with respective cardinals a,b,c,d defined by:

$$\begin{cases} A \coloneqq \{v_i \mid M_1(v_i) = 1, M_2(v_i) = 1\} \\ B \coloneqq \{v_i \mid M_1(v_i) = 1, M_2(v_i) = 0\} \\ C \coloneqq \{v_i \mid M_1(v_i) = 0, M_2(v_i) = 1\} \\ D \coloneqq \{v_i \mid M_1(v_i) = 0, M_2(v_i) = 0\} \end{cases} \tag{1}$$

Almost all common similarity measures (Sokal measure family, Sørensen-Dice, correlation etc.) can be defined with a,b,c,d. If one of the binary categorical variable can be considered as the truth, let's say M_2, therefore a becomes the number of *True Positives*, b of *False Positives*, c of *False Negatives* and d of *True Negatives*. We also trivially have the *Sensitivity*: $a/\left(a+c\right)$, *Specificity*: $d/\left(d+b\right)$, and the *Positive Predicted Value* (PPV): $a/\left(a+b\right)$. In fMRI, the v_i are the voxels and the variables M_1, M_2 are the functional maps to be compared (binary here, but the definition can easily be extended to probability maps).

3.2.1. Jaccard's index

When comparing two spatially distributed data, the most obvious measure is the Jaccard's index: the ratio between the size of their intersection and their union. It is defined by $J = a \,/\, (a + b + c)$ in our notation system. It provides intuitive and visual information about the overlap between one tested correlation map and one reference. It is also test-dependent: changing the risk or the multiple comparisons correction at the detection step will also change the shape and extent of the functional area, generally modifying Jaccard's index. This may be considered as a drawback but in fact, a statistical test is usually used at some point when investigating functional data.

3.2.2. Receiver operating characteristic analysis

In this section, we assume that the binary categorical variables are parameterized by at least one parameter. For example, in our case, it could be the risk for the statistical test of correlation α or a threshold on correlation r. Let r be our parameter, a_r, b_r, c_r, and d_r the previously defined cardinals in (1) now parametrized by r, and let define a set $\{(x(r), y(r)), r \in [-1, 1]\} \subset [0, 1]^2$ by:

$$\begin{cases} x(r) = 1 - \frac{d_r}{d_r + b_r} \\ y(r) = \frac{a_r}{a_r + c_r} \end{cases} \tag{2}$$

The implicitly defined function $f : x \mapsto y$ is called the *Receiver operating characteristic curve* (ROC-curve) and its integral $\int_0^1 f(x)dx$ is simply called the *Area Under Curve* (AUC). In the case where M_2 is considered to be the truth, f is just informally $f : 1 - Specificity \mapsto Sensitivity$. The AUC is not test-dependent as it covers all possible values of the threshold parameter (i.e. risk/correlation). It illustrates how a functional map *can* be close to the reference by considering *all* values of the considered parameter, while the Jaccard's index reflects how it *is* close to the reference by considering *one* value of the given parameter. Hence AUC is a better way to assess the trend of interest from a *theoretical* point of view. However, it is further away from the *practical* proximity of the Jaccard's index modeling offers, so we will eventually consider both scores.

3.3. Modeling trend with respect to the duration

Both Jaccard's index and AUC are computed for each subject, each seed, each duration and each functional network reference from MSDL. The next step is to model the trend of these two scores evolution according to the acquisition duration for all subjects and for each combination between one seed and one reference. Assuming rs-ASL sequence lasts long enough to cover all usage, extrapolation for a duration longer than 24 min 30 s seems superfluous. There is no theoretical model, even in BOLD, on the dependence between acquisition duration and quality of functional networks detection: we are not seeking for an explicit formula. Moreover, even processed independently, neighboring within-subject time-points have a strong dependency as they come from the same acquisition. Under these conditions, a local non-parametric regression is very well-suited. We chose to use the Loess method. Loess can be understood as a local polynomial regression on a subset of the whole dataset, defined by a weighted K-nearest neighbors algorithm. For a more comprehensive description, see (Cleveland and Devlin, 1988). We used second degree polynomial functions with a 0.8 span.

3.4. Data and code availability

In accordance with the consent form signed by the subjects, authors are not allowed to share MRI acquisitions. For the preprocessing steps we used Matlab CONN toolbox (www.nitrc.org/projects/conn, RRID:SCR_009550) (Whitfield-Gabrieli and Nieto-Castanon, 2012). The rest of the code used for evaluation scores and Loess is available upon request from the corresponding author.

4. Results

4.1. Optimal acquisition duration for the Default Mode Network

In this section, we present an in-depth analysis of the DMN. In the set of 20 seeds we used, many should not be inspected when used in combination with MSDL DMN. The main reason is that most of the combinations has no objective basis for detecting the DMN. Otherwise, the seed may have failed to detect precisely the networks it was meant to detect, which is expected with very short acquisition duration. A good way to get an idea of the quality of the overlap between the functional maps associated with a seed and a reference for all durations is to check the boxplots of the Jaccard's index as in Figure 2.

Boxplots give an overview of the results for rs-ASL: for the DMN reference, Jaccard's indices have higher values for the seeds placed in order to detect it. Prefrontal and posterior seeds seem to work well while lateral DMN seeds provide lower scores but still higher than any other seeds.

Figure 3 shows the evolution of the estimated DMN with the prefrontal seed. Three stages can be identified. First, at 2 min, the maps show only false positive noise detection. Next step, between 4 min and 10 min, this false positive has disappeared while the frontal component of the DMN starts growing. However, the lateral and posterior components are barely detected. Last step, after 10 min, the lateral and posterior components starts being detected. The functional maps look stabilized and well detected after 14 min. Figure 4 shows the Jaccard's index, AUC, Sensitivity and Predicted Positive Value (PPV), for each subject and at each acquisition duration. Loess on Jaccard's index, as well as on AUC, models quite well what can be observed by looking directly at the functional map. Jaccard's index seems to stabilize after 12-13 min and AUC at an earlier acquisition duration around 9-10 min. We could have expected sensitivity and PPV to follow the same trend. Actually, sensitivity just grows over time, but more slowly for longer durations. Interestingly, PPV reaches a peak in the second stage mentioned above. The seven subjects show different level of response but good correlations (except for the subject 2 with AUC), i.e. the trend is the same

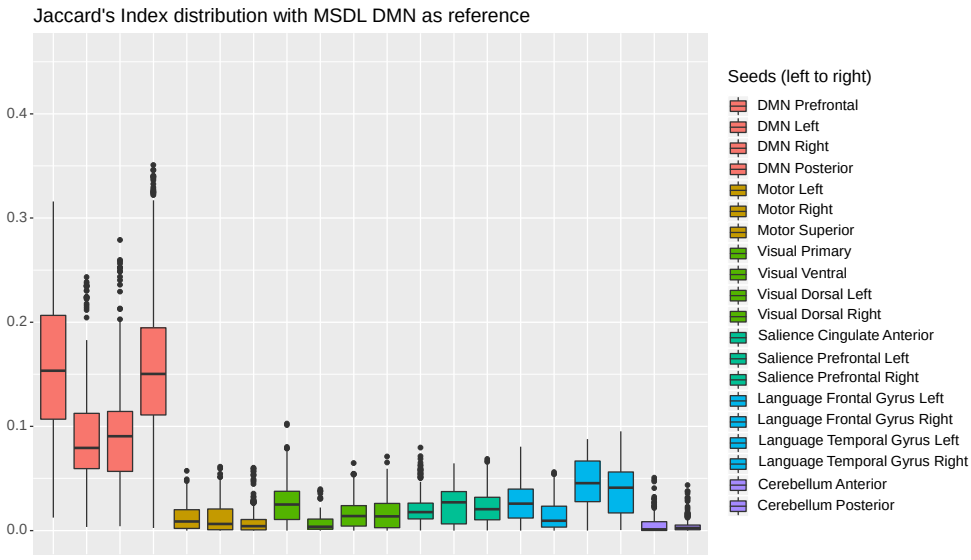

Figure 2: Each boxplot corresponds to one seed and shows the distribution of Jaccard's index between the estimated functional area corresponding to the considered seed on the one hand, and the MSDL DMN reference on the other hand, for all subjects and all durations. The seeds are grouped by color, each corresponding to one of the six functional areas considered. As expected, the seeds located in the expected DMN location (in pink) give the best results.

among subjects, rather than an average effect induced by the Loess. Moreover results observed for the DMN, can be generalized for almost every combination of seeds and references as we will see.

4.2. Optimal acquisition duration for all functional networks

Although visual inspection of acquisition and the estimated functional networks estimation is always a good practice (Power, 2017), there are more than 6000 functional maps generated (20 seeds, 7 subjects, 46 acquisition durations), we cannot check all of them. As seen for DMN, many combinations between seeds and reference should not be investigated since they will yield to very low overlapping scores. For Jaccard's index, we selected combinations for which at least 50% of observations have $J \geqslant 0.1$. For AUC, the median is also considered, with a threshold of 0.7. These thresholds on the median values may seem rather low, but let us remember that all the acquisition durations are taken into account,

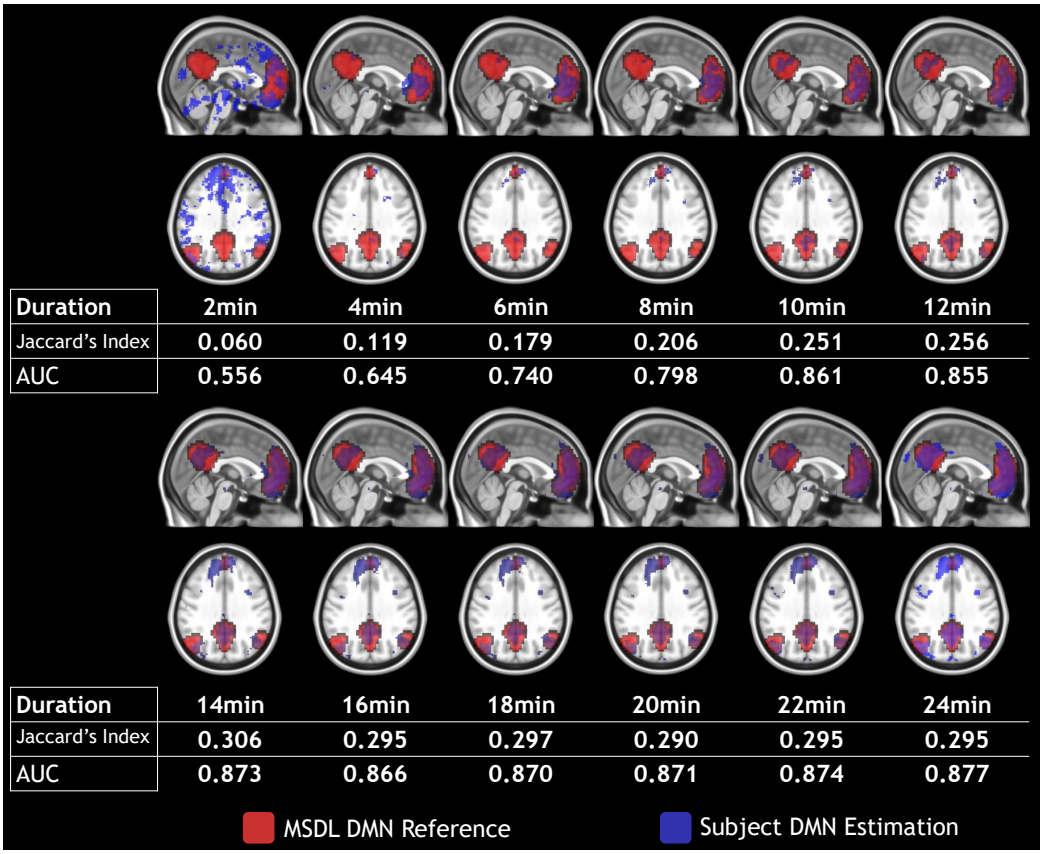

Figure 3: Subject 4 DMN detection (in blue) with prefrontal seed and MDSL DMN reference (in red) over a 2 min to 24 min duration with 2 min steps. Maps are shown in MNI152 space.

even the shortest ones. Figure 5 shows the median values for all the combinations between seeds and references. The two thresholds lead to an almost identical choice for the selection of combinations. All seeds have their best scores with the expected reference, and each of the six functional networks are considered to be sufficiently well detected with SBA for Jaccard's index in accordance with our selection rules. The AUC suggests as good enough one more seed for cerebellum but consider that salience is not detected well enough with our set of seeds.

Figure 6 shows the range of durations where scores are not significantly different from their maximum values (5% risk) for each selected reference/seed combination. Colors on heatmap are scaled between minimum and maximum values of the corresponding score and match with the stages already described for DMN in the previous section. Indeed, for every combination between seeds

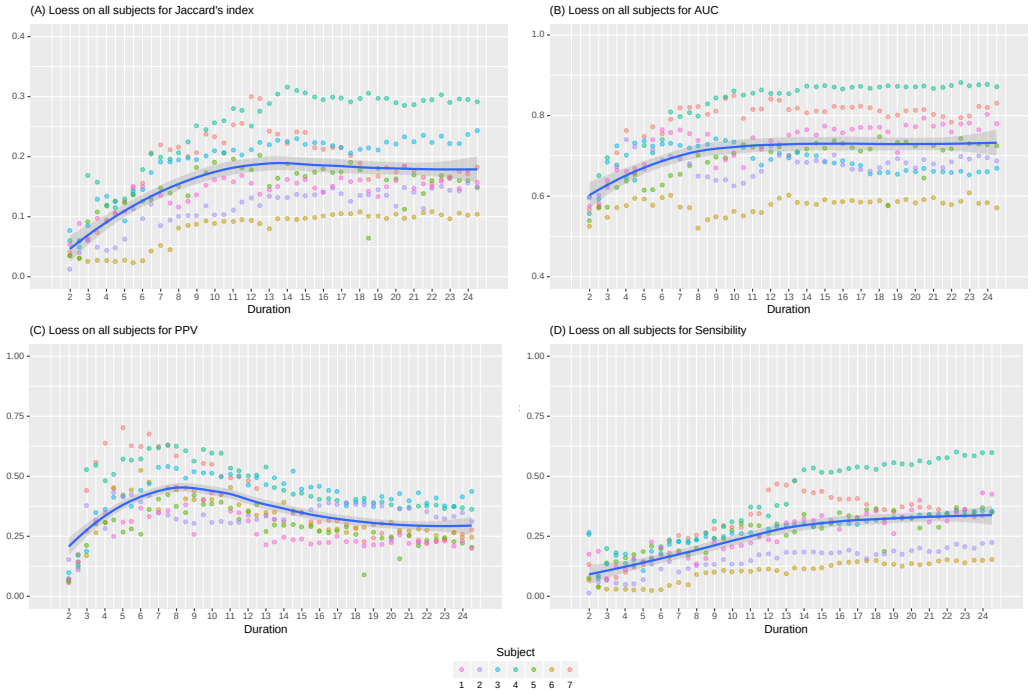

Figure 4: Jaccard's indices (A), AUC (B), Positive Predicted Value (C) and Sensibility (D) evolution with time with their associated Loess for the seed associated with prefrontal DMN. On all subjects, Jaccard's index increases with duration before 10-12 min, then stabilizes. The AUC shows the same trend with an earlier stabilization, around 8-10 min. PPV grows rapidly, reaches a peak at 8 min, then decreases slowly. Finally, Sensitivity increases with time, but more slowly for longer durations. Subjects show different level of response but good correlations.

and references, both scores rapidly increase, and start to stabilize after a certain duration. However, for both measures, the 95% confidence interval around the maximum suggests a later start in the stabilization than suggested directly by the Loess curve values. While some combinations scores look already stabilized at 12 min, almost all of them are close to their maximum value at 16 m. Figure 7 shows a collection of functional areas obtained at a duration of 14 min. While language seed struggles to detect spatial components far from the seeds, all the other ones provide good detection of expected functional networks. The two bottom rows show the same subjects and the same reference with different seeds.

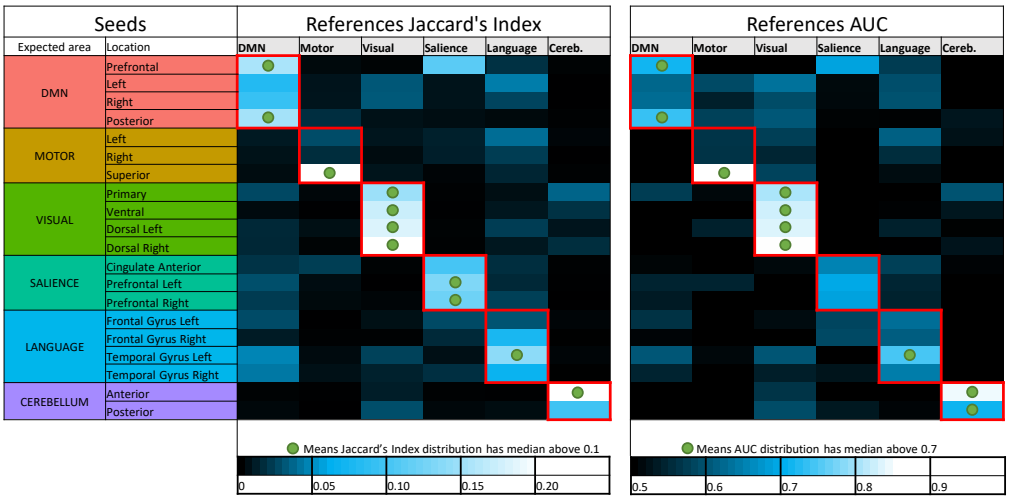

Figure 5: Median values of Jaccard's indices and AUC for all combinations of seeds/references. Green circles show where seeds/reference combinations are selected with respect to our thresholding rules (0.1 for the Jaccard median and 0.7 for the AUC median).

5. Discussion

5.1. On methods

In order to estimate functional networks, the two most common methods are SBA and Independent Component Analysis (ICA). We did not work with ICA because the association between independent components, obtained with ICA, and functional areas of the brain is intrinsically tedious (McKeown et al., 2003) (Cole et al., 2010), especially when it comes to comparison between subjects. Moreover, in order to investigate the relationship between quality and duration for all subjects, we must estimate the functional areas in the same way for each subject. Indeed, keeping the same seeds and the same test for SBA is trivial, while keeping the same number of independent components is equivocal, since it should be decided by a goodness of fit criterion.

We chose to report the positive predicted value rather than specificity for two main reasons. On the one hand, true negatives can have multiple definitions in fMRI, since it depends on the voxels considered: the whole volume, only the brain or any smaller ROI like grey matter. Although it is logical to consider only brain voxels for functional activity, this implies an extremely high number of true negatives, since the volume of a functional network is ten to a hundred times smaller than the one of the whole brain. Therefore, the specificity reaches

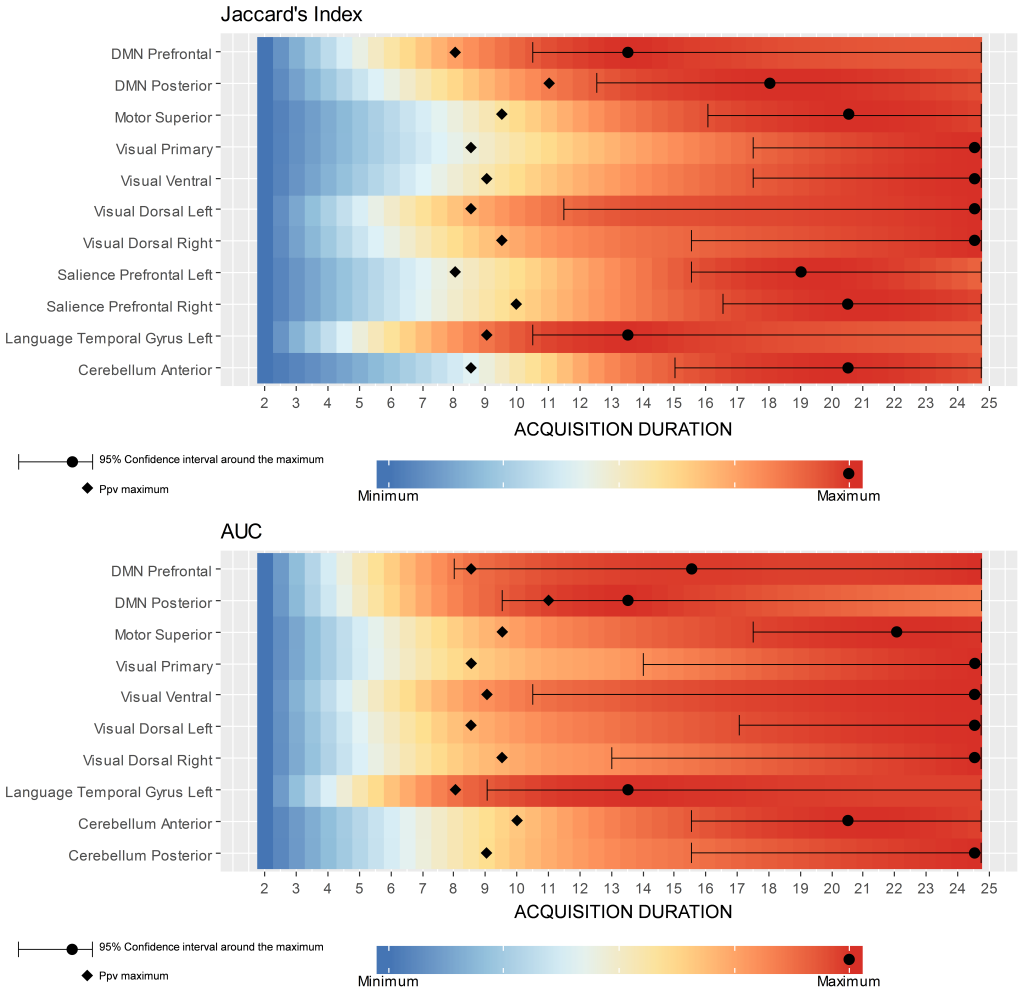

Figure 6: Color maps of Jaccard's Index and AUC Loess value with respect to the acquisition duration for all selected reference/seed combination. Every combination has a fast increasing score followed by a stabilization stage. The PPV peak shows on all combinations around 9 min and appears always just before score start stabilizing. Maximum and its 95% confidence interval may be unstable since score variations are often low after PPV peak.

values too high to provide relevant information on similarity between functional areas. On the other hand, like specificity, PPV plays a similar role with respect to sensitivity: specificity gives a complementary information to sensitivity in the

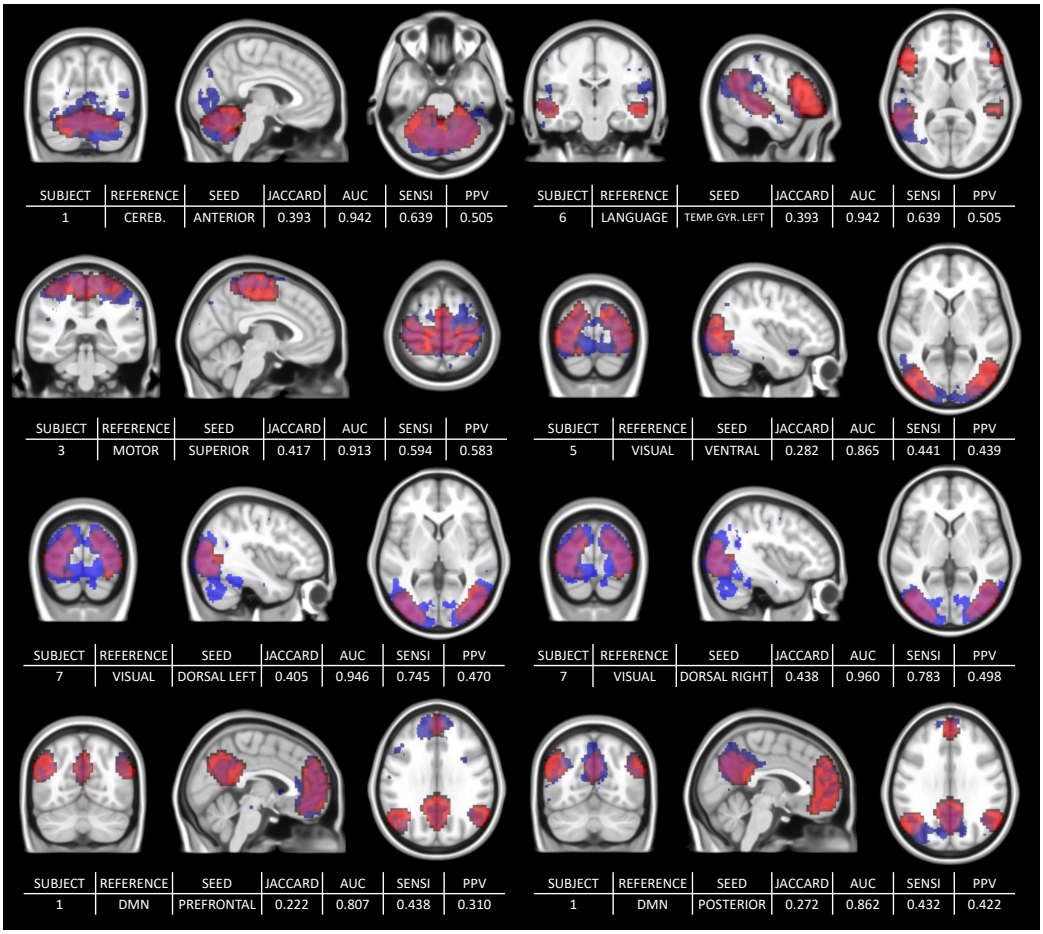

Figure 7: Collection of functional areas at 14 min with the corresponding scores: Jaccard's Index, Area Under the Curve, Sensitivity and PPV. The two bottom rows show the same subjects and the same reference but with different seeds. The third row shows the estimated (blue) and reference (red) visual network for the same subject (subject 7) but different seeds ("dorsal left" seed on the left and "dorsal right" seed on the right). Similarly, the bottom row shows the same subject (subject 1) with different seeds ("Prefrontal" and "Posterior")

totality of voxels whereas PPV gives a complementary information in the union of the reference and the estimated functional area.

5.2. On results

Our two objectives were to confirm the feasibility of resting state ASL and to evaluate the influence of the acquisition duration on the estimation of functional areas. Figure 3 and Figure 7 with corresponding scores in Figure 5 and in Figure 6

confirm that, even with the basic preprocessing and straightforward methodology we used, ASL is fully viable as a resting-state method. Regarding the optimal duration, we show the stabilization of the functional areas representation after a certain duration for both measures, Jaccard's index and AUC, with a strong inter-subjects correlation (i.e. not a mean-effect induced by the Loess modeling). Since the acquisition should have the shortest duration possible for clinical implementation, the recommended duration eventually corresponds to the start of the stabilization stage. Strict definitions of the stabilization stage, lead to longer duration since they would rely heavily on the Loess maximum by considering as stable just a narrow interval around of the maximum. However, since after 12 min to 14 min the score variations are low, a slight change in preprocessing or in the population could also lead to unstable maximum, without changing the trend. Relaxed definitions would keep optimal duration stability, but they may consider a functional area as good enough when an human investigator would not. Actually, early stages of acquisition are associated with poor representation of functional areas disconnected from the seed.

Based on our different results, 14 min seems to be an interesting compromise regarding the optimal acquisition time. Note that the DMN, the sensori-motor cortex and the cerebellum have an almost consensual spatial definition among the authors, unlike language, visual and salience, which show a greater spatial variability (see for example http://neurosynth.org/). As we provide an evaluation only with one set of references (from the MSDL), one could have expected this to be a major limitation of our work. However the spatial variability of the areas of interest in atlases is low enough to not critically change the trend observed in this paper. Preprocessing influence should also be considered as positive: since we use typical and basic preprocessing, more advanced techniques should provide the same or a shorter optimal duration. Not to mention the resting state, ASL is very sensitive to changes in its parameters. Since we are studying the influence of acquisition duration for a given set of parameters, the optimal duration of 14 min could be strongly influenced by the sequence parameters. Although the influence of each of them is to be kept in mind, most of them should not disturb the investigators, as most of them have a specific bibliography that goes well beyond the issue of the optimal acquisition duration. However, two of them may have a deep impact on our results: post-labeling delay and repetition time (TR). As mentioned in section 2.2, we already have some clues on how the PLD can influence functional networks representation. The critical parameter in our opinion is repetition time. It defines the sample frequency of the resting-state signal and turning our 14 min suggestion into a 240 volumes since we only work

numerically on the signal. Its variation may widely shift the stabilization step toward a higher/lower number of volumes and hence a longest/shortest duration, without changing the stabilization of the functional networks representation after a certain number of volume (i.e. same signal but different sampling frequency). Moreover in rs-ASL, TR values are typically between 3 s and 5 s, which is too wide to assume the locally linear dependence between TR and optimal duration. As a preliminary work on optimal duration in rs-ASL, we focus more on the modeling rather than investigating the influence of the TR. However, a specific study on the relationship between repetition time, number of volumes and quality of acquisition would be, in our opinion, highly beneficial to better define the optimal duration and also would be useful when an investigator set up a sequence.

6. Conclusion

We model and process data in order to get results as close as an investigator would do. All the considered functional areas were well detected by rs-ASL. Our results show a quality stabilization after a certain duration for both scores in all but one combination between seeds and references: very long sequences should not hence be considered. As discussed, we would eventually recommend a 14 min duration for TR = 3500ms / 240 volumes: it seems to be a good balance between strict and relaxed definitions of where the stabilization starts. The exploration of the influence of sequence parameters, especially the TR, on the optimal duration was beyond the scope of this article but would be highly beneficial for sequence implementation. Variations induced by a change in references could be a future work, but rather in the context of a study on atlases than specifically on the issue of acquisition duration.

Acknowledgement

MRI data acquisition was supported by the Neurinfo MRI research facility from the University of Rennes I. Neurinfo is granted by the the European Union (FEDER), the French State, the Brittany Council, Rennes Metropole, Inria, Inserm and the University Hospital of Rennes.

Conflict of interest

None

Appendix - Seed location in MNI152

Expected networks	Seed	Location in MNI152
DMN	Prefrontal	(1,55,-3)
DMN	Left	(-39,-77,33)
DMN	Right	(47,-67,29)
DMN	Posterior	(1,-61,38)
Motor	Left	(-55,-12,29)
Motor	Right	(56,-10,29)
Motor	Superior	(0,-31,67)
Visual	Primary	(2,-79,12)
Visual	Ventral	(0,-93,-4)
Visual	Dorsal Left	(-37,-79,10)
Visual	Dorsal Right	(38,-72,13)
Salience	Cingulate Anterior	(0,22,35)
Salience	Prefrontal Left	(-32,45,27)
Salience	Prefrontal Right	(32,46,27)
Language	Frontal Gyrus Left	(-51,26,2)
Language	Frontal Gyrus Right	(54,28,1)
Language	Temporal Gyrus Left	(-57,-47,15)
Language	Temporal Gyrus Right	(59,-42,13)
Cerebellum	Anterior	(0,-63,-30)
Cerebellum	Posterior	(0,-79,-32)

Bibliography

Agosta, F., Pievani, M., Geroldi, C., Copetti, M., Frisoni, G. B., and Filippi, M. (2012). Resting state fMRI in Alzheimer's disease: Beyond the default mode network. *Neurobiology of Aging*, 33(8):1564–1578.

Alsop, D., Detre, J., Golay, X., Günther, M., Hendrikse, J., Hernandez-Garcia, L., Lu, H., Macintosh, B., Parkes, L., Smits, M., Van Osch, M., Wang, D., Wong, E., and Zaharchuk, G. (2015). Recommended implementation of arterial spin-labeled Perfusion mri for clinical applications: A consensus of the ISMRM Perfusion Study group and the European consortium for ASL in dementia. *Magnetic Resonance in Medicine*, 73(1):102–116.

Alsop, D. C., Dai, W., Grossman, M., and Detre, J. A. (2010). Arterial Spin Labeling Blood Flow MRI: Its Role in the Early Characterization of Alzheimer's Disease. *Journal of Alzheimer's Disease*, 20(3):871–880.

Behzadi, Y., Restom, K., Liau, J., and Liu, T. (2007). A component based noise correction method (CompCor) for BOLD and perfusion based fMRI. *NeuroImage*, 37(1):90–101.

Birn, R., Molloy, E., Patriat, R., Parker, T., Meier, T., Kirk, G., Nair, V., Meyerand, E., and Prabhakaran, V. (2013). The effect of scan length on the reliability of resting-state fMRI connectivity estimates. *NeuroImage*.

Biswal, B., Yetkin, Z., Haughton, V., and Hyde, J. (1995). Functional connectivity in the motor cortex of resting human brain using echo-planar MRI. *Magnetic resonance in medicine : official journal of the Society of Magnetic Resonance in Medicine / Society of Magnetic Resonance in Medicine*, 34(4):537–41.

Boissoneault, J., Letzen, J., Lai, S., O'Shea, A., Craggs, J., Robinson, M., and Staud, R. (2016). Abnormal resting state functional connectivity in patients with chronic fatigue syndrome: An arterial spin-labeling fMRI study. *Magnetic Resonance Imaging*, 34(4):603–608.

Borogovac, A. and Asllani, I. (2012). Arterial spin labeling (ASL) fMRI: Advantages, theoretical constrains and experimental challenges in neurosciences. *International Journal of Biomedical Imaging*, 2012.

Bouix, S., Swago, S., West, J. D., Pasternak, O., Breier, A., and Shenton, M. E. (2017). Evaluating Acquisition Time of rfMRI in the Human Connectome

Project for Early Psychosis. How Much Is Enough? Number 2017, pages 108–115.

Buxton, R., Frank, L., Wong, E., Siewert, B., Warach, S., and Edelman, R. (1998). A general kinetic model for quantitative perfusion imaging with arterial spin labeling. *Mag. Res. Med.*, 40(3):383–396.

Chen, J., Jann, K., and Wang, D. (2015). Characterizing Resting-State Brain Function Using Arterial Spin Labeling. *Brain Connectivity*, 5(9):527–542.

Cleveland, W. S. and Devlin, S. J. (1988). Locally Weighted Regression: An Approach to Regression Analysis by Local Fitting. *Journal of the American Statistical Association*, 83(403):596.

Cole, D., Smith, S., and Beckmann, C. (2010). Advances and pitfalls in the analysis and interpretation of resting-state FMRI data. *Frontiers in systems neuroscience*, 4(April):8.

Craddock, C., Holtzheimer, P., Hu, X., and Mayberg, H. (2009). Disease state prediction from resting state functional connectivity. *Magnetic Resonance in Medicine*, 62(6):1619–1628.

Eklund, A., Nichols, T., and Knutsson, H. (2016). Cluster failure: Why fMRI inferences for spatial extent have inflated false-positive rates. *Proceedings of the National Academy of Sciences*, 113(33):E4929–E4929.

Gao, L. and Wu, T. (2016). The study of brain functional connectivity in Parkinson's disease. *Translational Neurodegeneration*, 5(1):1–7.

Grade, M., Hernandez Tamames, J. A., Pizzini, F. B., Achten, E., Golay, X., and Smits, M. (2015). A neuroradiologist's guide to arterial spin labeling MRI in clinical practice. *Neuroradiology*, 57(12):1181–1202.

Liang, X., Connelly, A., and Calamante, F. (2014). Graph analysis of resting-state ASL perfusion MRI data: Nonlinear correlations among CBF and network metrics. *NeuroImage*, 87:265–275.

Liang, X., Tournier, J., Masterton, R., Connelly, A., and Calamante, F. (2012). A k-space sharing 3D GRASE pseudocontinuous ASL method for whole-brain resting-state functional connectivity. *International Journal of Imaging Systems and Technology*, 22(1):37–43.

Lynall, M.-E., Bassett, D. S., Kerwin, R., McKenna, P. J., Kitzbichler, M., Muller, U., and Bullmore, E. (2010). Functional Connectivity and Brain Networks in Schizophrenia. *Journal of Neuroscience*, 30(28):9477–9487.

McKeown, M., Hansen, L., and Sejnowski, T. (2003). Independent component analysis of functional MRI: What is signal and what is noise? *Current Opinion in Neurobiology*, 13(5):620–629.

Mutsaerts, H., Nordhøy, W., Pizzini, F., van Osch, M., Zelaya, F., Hendrikse, J., Wastling, S., Petersen, E., Günther, M., Wang, Y., Geier, O., Fernandez-Seara, M., Golay, X., Wang, D., Fallatah, S., Nederveen, A., Groote, I., and Bjørnerud, A. (2015). Multi-vendor reliability of arterial spin labeling perfusion MRI using a near-identical sequence: Implications for multi-center studies. *NeuroImage*, 113:143–152.

Power, J. (2017). A simple but useful way to assess fMRI scan qualities. *NeuroImage*, 154(June 2016):150–158.

Van den Heuvel, M. and Hulshoff Pol, H. (2010). Exploring the brain network: A review on resting-state fMRI functional connectivity. *European Neuropsychopharmacology*, 20(8):519–534.

Varoquaux, G., Gramfort, A., Pedregosa, F., Michel, V., and Thirion, B. (2011). Multi-subject dictionary learning to segment an atlas of brain spontaneous activity. *Lecture Notes in Computer Science (including subseries Lecture Notes in Artificial Intelligence and Lecture Notes in Bioinformatics)*, 6801 LNCS:562–573.

Wang, D. J., Alger, J. R., Qiao, J. X., Hao, Q., Hou, S., Fiaz, R., Gunther, M., Pope, W. B., Saver, J. L., Salamon, N., and Liebeskind, D. S. (2012). The value of arterial spin-labeled perfusion imaging in acute ischemic stroke: Comparison with dynamic susceptibility contrast-enhanced MRI. *Stroke*, 43(4):1018–1024.

Whitfield-Gabrieli, S. and Nieto-Castanon, A. (2012). Conn : A Functional Connectivity Toolbox for Correlated and Anticorrelated Brain Networks. *Brain Connectivity*, 2(3):125–141.

Wolk, D. A. and Detre, J. A. (2012). Arterial spin labeling MRI: An Emerging Biomarker for Alzheimer's Disease and Other Neurodegenerative Conditions. *Current Opinion in Neurology*, 25(4):421–428.

Zhang, N., Gordon, M., and Goldberg, T. (2016). Cerebral blood flow measured by arterial spin labeling MRI at resting state in normal aging and Alzheimer's disease. *Neuroscience & Biobehavioral Reviews*, 72:168–175.

Zhou, D., Thompson, W., and Siegle, G. (2009). MATLAB toolbox for functional connectivity. *NeuroImage*, 47(4):1590–1607.